International Journal of Mass Spectrometry 335 (2013) 45–56

Contents lists available at SciVerse ScienceDirect

International Journal of Mass Spectrometry

journal homepage: www.elsevier.com/locate/ijms

A high-resolution gas-source isotope ratio mass spectrometer

John M. Eiler[a,*], Matthieu Clog[a], Paul Magyar[a], Alison Piasecki[a], Alex Sessions[a], Daniel Stolper[a], Michael Deerberg[b], Hans-Juergen Schlueter[b], Johannes Schwieters[b]

[a] Division of Geological and Planetary Sciences, California Institute of Technology, United States
[b] Bremen Mass Spectrometry group, ThermoFisher, United States

ARTICLE INFO

Article history:
Received 24 August 2012
Received in revised form 16 October 2012
Accepted 17 October 2012
Available online 23 October 2012

Keywords:
Stable isotope
Geochemistry
Hydrocarbon

ABSTRACT

We describe a new high-resolution, multi-collector gas source mass spectrometer designed for isotopic analysis of volatile and semi-volatile molecules: the Thermo Scientific MAT253-Ultra, a prototype double-focusing isotope ratio mass spectrometer installed in the Caltech laboratories for stable isotope geochemistry. This instrument achieves mass resolving power of up to ~27,000 ($M/\Delta M$) and can analyze diverse gases and semi-volatile compounds using a conventional dual inlet and/or a carrier gas. It has a multi-collector array comprised of 7 detector positions with adjustable spacing, all of which can register ions through an SEM or Faraday cup and spanning up to a 10^{13} range in signal strength. Abundance sensitivity in the He mass range is as good as 10^{-12}, and precision commonly approaches the counting statistics limit down to 0.1‰ (SEM) or 0.01‰ (Faraday) for a range of analytes. This instrument permits resolution of isobaric interferences arising from both contaminants and multiple isotopologues of an analyte that share a cardinal mass, enabling direct isotopic analysis of molecules with complex mass spectra such as hydrocarbons. This ability should enable the measurement of position-specific isotopic compositions, including multiple substitutions, by comparing isotope ratios of molecular ions with those of daughter fragment ions (assuming products of recombination and other source reactions are recognized and corrected for). The combination of high mass resolution with stable multicollection will provide a wide range of potential new tools for isotope geochemistry, including (but not limited to): singly and multiply substituted methane and larger hydrocarbons; position-specific ^{13}C analysis of propane and larger hydrocarbons; precise analysis of $^{17}O/^{16}O$ and $^{18}O/^{16}O$ on fragment ions from CO_2 and other molecules; analysis of a variety of N_2O isotopologues (including ^{18}O, ^{17}O, position-specific ^{15}N, and various 'clumped' species); and high precision and abundance sensitivity noble gas analyses. These capabilities greatly extend the scope of stable isotope variations that can be utilized for problems in forensics, environmental geochemistry, biochemistry, and Earth and planetary sciences.

1. Introduction

The gas source, multi-collector isotope-ratio mass spectrometer (IRMS) is the basis for most stable isotope analyses of volatile compounds containing the elements H, C, N, O and S. The study of stable isotopes is routinely applied to a variety of fields in the natural sciences including forensics, biomedical research, and other disciplines (e.g., [1–6]). Such instruments have a number of important strengths: (1) their Nier-type electron impact (EI) ion sources generate bright (nA to μA) and stable ion beams; (2) their multiple-collector arrays permit highly precise (down to ppm) measurements of small relative differences in isotopic compositions; and (3) the dual viscous-bleed inlet systems used on many gas source IRMS's permit rapid comparison of sample and standard under essentially identical instrument conditions, providing exceptional accuracy (i.e., relative to a defined standard reference frame [7–10]). Perhaps the greatest testament to the success of these instruments is that they have changed relatively little in basic design and performance since their creation nearly 70 years ago.

However, existing gas source IRMS's have a number of weaknesses that limit the scope of isotopic variations they can measure: (1) their analytes must be gases—generally low-molecular weight compounds with high vapor pressure at room temperature—or sufficiently volatile to be delivered to the EI ion source in a carrier gas; (2) existing commercial IRMS's detect ions only through Faraday cups, which are noteworthy for their linearity and stability but have relatively large background currents (~fA) that restrict minimum detection limits. Minimum sample sizes of 10s of picomoles have been analyzed by carrier gas mass spectrometry (a.k.a. continuous-flow IRMS or isotope-ratio-monitoring MS [11]), and isotopologues as rare as ~tens of ppm, relative, have been measured precisely in IRMS's configured for clumped isotope analyses (i.e.,

* Corresponding author. Tel.: +1 626 395 6942.
E-mail address: eiler@gps.caltech.edu (J.M. Eiler).

1387-3806/$ – see front matter © 2012 Elsevier B.V. All rights reserved.
http://dx.doi.org/10.1016/j.ijms.2012.10.014

measurements of species containing two or more rare isotopes) of CO_2 [12,13]. Nevertheless, the Johnson noise inherent in Faraday cup amplifiers means that little more can be done to extend these limits further without employing high-sensitivity, low noise detectors such as secondary electron multipliers (SEM's). (3) Modern IRMS instruments have low mass resolving power—significantly lower than the most sophisticated thermal, plasma and secondary ion mass spectrometers. Hereafter, unless otherwise noted, mass resolution is defined as mass (M) divided by the width, in equivalent mass units, of the ion beam (ΔM), calculated as the central portion of the beam containing 90% of its current; this is also referred to as the '5–95% definition' of mass resolving power. Mass resolution of commercial IRMS instruments vary by design, tuning, and analyte, but is typically on the order of ~200 for gases of moderate molecular mass (N_2, O_2, CO_2, etc.; for comparison, double-focusing sector mass spectrometers commonly achieve mass resolutions of ~10,000). This comparatively low resolution means these instruments are generally incapable of distinguishing target analyte ions from isobaric interferences, including both contaminant gases (e.g., $H^{16}O$ and $^{13}CH_4$ at 17 amu or $^{13}C^{16}O_2{}^+$ and $^{12}C^{16}O_2H^+$ at 45 amu) and isotopologues of the same gas that share a cardinal mass (e.g., $^{13}CH_4$ and $^{12}CH_3D$; we refer to these as 'isotopic isobars'). For this reason, IRMSs are generally only used to measure a few specific analytes that can be easily purified, do not have significant isobaric interferences with ubiquitous vacuum contaminants, and are sufficiently simple in stoichiometry that ion-correction schemes can deconvolve at least some of their isotopic isobars. CO_2, H_2, N_2 and O_2 are widely studied; SO_2, SF_6 and N_2O are analyzed in a smaller number of specialized laboratories; CO is increasingly targeted as an analyte in the effluent of on-line pyrolysis; and SiF_4 has been an occasional target of specialized laboratories. This is effectively the full scope of IRMS analyses in stable isotope geochemistry.

In contrast, geochemists studying the isotopes of heavier elements have traditionally analyzed a wider array of analytes, containing elements with many isotopes that cover broader and often overlapping mass ranges. These analyses often encounter more severe isobaric interferences and problems of abundance sensitivity. To deal with these problems, mass spectrometers have been developed for this community that employ thermal ionization (TIMS) or inductively coupled plasma (ICP) ion sources coupled to more sophisticated mass analyzers as compared to gas source IRMSs. These improved capabilities include higher mass resolving power (up to $M/\Delta M$ of ~10,000), moveable detector arrays of both Faraday cups and SEMS, multiplexed Faraday cups and amplifiers that allow rapid switching of gain, and energy-filtering lenses (e.g., the retardation potential quadrupole, RPQ, on Thermo instruments) at the detector array to improve abundance sensitivity. However, the plasma ion source of ICP-MS instruments make them ill suited to analyses of volatile light elements that are components of air, water and organic matter (i.e., H, C, N, O and the noble gases; an exception is S, which has been successfully analyzed by multi-collector ICP-MS [14]). Additionally, the relatively slow sample/standard comparisons (order of minutes), memory washout effects and comparatively unstable sources of TIMS and ICP-MS instruments make it difficult to achieve the high precision reachable with conventional gas source IRMS's (as good as ~5–10 ppm compared to ~100 ppm on TIMS and ICP-MS). Finally, and most importantly for our purposes, the plasma torch of ICP-MS instruments ionize under such energetic conditions that it is unlikely any molecular species can survive with original intramolecular bonds intact. Thus, these instruments are intrinsically not appropriate for clumped isotope analyses or measurements of other intramolecular isotope effects, such as position-specific isotope analyses (e.g., the position specific ^{15}N of N_2O [15]).

Several other approaches to mass spectrometry (e.g., reverse geometry, double-focusing sector instruments; tandem mass spectrometers; ion cyclotron resonance, time-of-flight, and 'orbitrap' mass analyzers) achieve exceptionally high mass resolution (~100,000 or greater), sufficient to discriminate a wide range of isobaric interferences, including both contaminants and virtually all isotopic isobars (e.g., [16]). However, no existing instrument of this kind has the combination of a stable, bright EI source, multi-collector array covering a large dynamic range, and dual inlet sample introduction that are fundamental to the exceptional precision and accurate standardization typical of IRMS instruments and required for most studies of natural stable isotope distributions.

Infrared absorption spectroscopy has recently emerged as an important complement to—and, in some cases, replacement for—IRMS measurements (e.g., [17]). This technique provides field-portability and lower cost for isotopic measurements of some species (e.g., CO_2 and N_2O), and has added to the list of molecules that can be directly analyzed (e.g., H_2O and CH_4). These methods may be extended to other volatile molecules. However, the low vapor pressure and vibrational complexity of larger species may make them more difficult analytes for precise isotopic analysis via infrared spectroscopy. Furthermore, there are no examples of absorption spectroscopy being used to make measurements of multiply substituted isotopologues (e.g., $^{13}C^{18}O^{16}O$, which makes up only ~46 ppm of natural CO_2) with the level of precision achieved by IRMS measurements and required for most studies of natural materials.

Finally, NMR analysis has been developed for measuring the $^{13}C/^{12}C$ and D/H ratios of specific atomic sites in organic compounds (e.g., [18–20]). These techniques hold great promise for studying the isotopic anatomy of complex organic structures (e.g., [21]) but are not yet widely used. Technical limitations of isotopic analysis by NMR currently include relatively low precision (~1 per mil), large (mg or more) sample sizes, and long integration times (often 24 h or longer). Sensitivity is perhaps the biggest limitation of NMR for our goals, because for many analytes it effectively prevents the measurement of very rare, multiply substituted species.

This paper presents the design, performance characteristics, and some representative applications of the Thermo Scientific MAT253-Ultra, a prototype high-resolution IRMS designed to overcome many of the limitations of existing commercial instruments. This instrument was created to enable precise, well-standardized analyses of isotope ratios based upon the mass spectra of a wide range of gases and volatile organic compounds (without conversion to a common form such as CO_2), and in particular to meet the challenges of analyzing multiply substituted species and position-specific isotope effects in compounds of H, C, N, O and S. It is also a highly capable instrument for noble gas analysis and possibly for high-precision measurements of concentration ratios in air or other gases.

2. The Thermo Scientific IRMS MAT 253-Ultra

The Thermo Scientific MAT253-Ultra (hereafter 'Ultra') is a gas source, double-focusing sector mass spectrometer that shares many design elements and components with several existing instruments: The inlet system and ion source are adapted from the Thermo Scientific MAT 253 IRMS, which has been widely used for high precision clumped isotope measurements of CO_2 and O_2 (e.g., [22]); the adjustable analyzer entrance slits are developed from those used in the Thermo Scientific Element 2 and Neptune Plus ICP-MSs; the electrostatic analyzer power supply was developed to obtain a higher stability than previously established for that used in the Thermo Neptune Plus ICP-MS; the proven magnetic sector technology, quadrupole focusing lenses and array of moveable detectors are adopted directly or modified from similar components of the Thermo Scientific Triton TIMS and Neptune Plus

ICP-MS; and the computer user interface is based upon Thermo's existing Isodat software, modified to allow it to run the Ultra. This software package has been developed over decades to meet the needs of stable isotope ratio measurements using gas source mass spectrometers. The Ultra incorporates nearly all improvements in multicollector TIMS and ICP-MS instrumentation over the last 2 decades, including multiple ion counting, moveable collectors, switchable current amplifier technology, ultra high vacuum, double focusing to enable high mass resolution and high abundance sensitivity.

Fig. 1 presents a schematic overview of the layout of the Ultra. Here we summarize its important design features, emphasizing modifications from existing, commercial instruments.

2.1. Inlet system

Analytes that have significant vapor pressures (~10s of mbar or more) at room temperature can be held in one of four automated compressible mechanical bellows (3–40 ml internal volume) identical to those in the Thermo Scientific MAT253, each of which delivers gas to the ion source through a separate metal capillary with the flow limited by a mechanical constriction (i.e., crimp). These capillaries are connected to the ion source by a changeover valve block—a set of pneumatic valves that can be cycled among several configurations, each of which permits the effluent from one capillary to enter the ion source while directing all others to a vacuum waste pump. This set of valves and associated computer control system is based on that used in the Thermo Scientific MAT 253 and Isodat. Four, rather than the standard two, bellows are included on the Ultra to help perform measurements that require complex standardization constrained by comparison of a sample with several standards, e.g., clumped isotope measurements where one must account for mass discrimination, fragmentation and H-transfer reactions in the source, the linearity of detectors, and perhaps other phenomena.

Analytes can also be delivered to the ion source via a carrier gas stream conducted through fused-silica capillaries and an open split, just as in conventional continuous-flow applications of other IRMS instruments. This capillary bypasses the changeover block and enters the source directly, and can be closed via a needle valve located just prior to the ion source. Flow rates accepted by the ion source are similar to other Thermo IRMS instruments, such that existing peripheral devices (e.g., Gas Bench, Conflo, and elemental analyzer) can be used without modification. As the capillaries are not heated in the current prototype, analytes are presently restricted to those with significant vapor pressure at room temperature. We intend to publish a separate study of the performance of the Ultra for continuous flow measurements in the near future, but our initial experiments with this configuration suggest basic performance characteristics (mass resolution, abundance sensitivity and precision) are broadly similar for CO_2 measured as a component of a He flow as for pure CO_2 measured using the dual inlet system (mass resolution and abundance sensitivity may be degraded by ~10–20%, relative).

2.2. Ion source

The ion source of the Ultra is an electron-impact ionization chamber closely resembling the Nier-type source long used in IRMS instruments [7]. It is based on the EI source of the Thermo Scientific MAT253, modified for the Ultra in three significant ways: (1) the overall length of the source has been reduced to make it compatible with the adjustable source slit and to maintain the source slit in its optimum position; (2) the mechanical aperture that controls the dynamic pumping speed of the ion source (often referred to as the 'sulfur window') has been re-engineered to be compatible with the space required by the adjustable slit arrangement; (3) the range of electron impact energies that can be achieved, defined by the voltage potential between the source filament and housing of the ionization chamber, has been extend to 25–150 eV rather than the standard range of 50–150 eV. This provides improved control over the fragmentation of molecular ions, and can be reduced further if needed.

2.3. Ion extraction and mass spectrometer entrance slits

The ion beam generated in a conventional Thermo Scientific MAT253 is electrostatically extracted, accelerated to 10 keV, focused, and passed through a 500 μm-wide mechanical aperture ('slit') that defines the entrance to the mass analyzer. Modifications to the extraction optics and entrance slit in the Ultra include: (1) The accelerating potential between the ion source and entrance slit is 5 keV, rather than 10 keV. This was done in order to achieve the double focusing condition with a compact electrostatic sector; (2) any one of three analyzer entrance slits can be selected under computer control. These slits, varying between 5 and 250 μm width, are mounted on a single physical 'slit tongue' which is pneumatically articulated. The slit-tongues are identical to those used on the Thermo Scientific Element 2 and Neptune Plus ICP-MS's. (3) The 'deflector' lenses immediately before and after the entrance slit have been replaced with quadrupole lenses for improved correction of ion beam rotation and stigmation.

The reduction in entrance slit width exerts the primary control over mass resolution by fixing the ion beam width at the image plane of the mass spectrometer (i.e., the detector array). For a fixed analyzer geometry, reduction in ion beam width means adjacent ion beams that are separated from one another by larger multiples of their widths at the image plane. I.e., ΔM becomes smaller and thus higher values of $M/\Delta M$ can be achieved. This strategy is straightforward and results in unprecedented mass resolution for a normal geometry sector instrument the scale of the Ultra. However, a smaller entrance slit produces a narrower ion beam by rejecting much of the primary beam, resulting in a corresponding loss of ion transmission and thus sensitivity. This trade-off and its implications for applied measurements are discussed at length below.

2.4. Electrostatic analyzer, magnet and transfer optics

The Ultra's mass analyzer is a double-focusing, normal geometry sector design (Fig. 1) in which the ion beam passes through an electrostatic analyzer (ESA) prior to entering the magnetic field. The energy dispersion of the ESA is designed to precisely compensate for the energy dispersion of the following magnetic sector in the double focusing condition. The Ultra's ESA has a radius of curvature of 22 cm and energy window of ~25 eV. Immediately after exiting the ESA, the ion beam is accelerated to 10 keV with respect to ground. This acceleration between ESA and magnet allows use of a compact ESA geometry—roughly a factor of 2 smaller than would be required if ions achieved their full 10 keV energy before entering the ESA. The compact ESA results in a relatively modest overall footprint for the Ultra (~1.5 m × 4 m, including electronics cabinets that fit within the instrument frame). The ion beam then passes through rotation and focusing quadrupole lenses before entering the magnet—a 23 cm radius, 90° sector electromagnet, controlled by feedback from a field probe. After exiting the magnet, the ion beam passes through another focusing quadrupole before reaching the detector array. The two focusing quadrupoles (i.e., just before and just after the magnet) can be tuned together to achieve a 'zoom optic' capability, permitting electrostatic expansion or compression of the mass dispersion by ~5%, relative, at the image plane

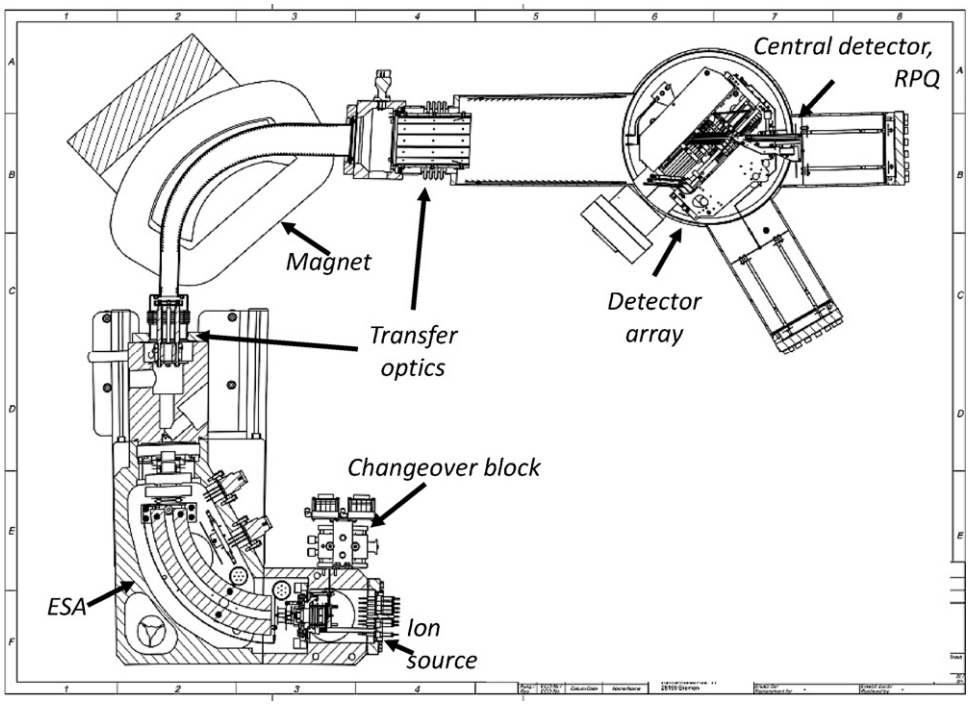

Fig. 1. Schematic illustration of the major components of the source, analyzer and detector array of the Thermo 253-Ultra. The changeover block is a set of pneumatic valves through which one of the 5 possible streams of analyte gas or carrier gas flows to the ion source. Other major labeled components include the Nier type electron impact ion source, the electrostatic analyzer (ESA), magnet and detector array. Not to scale.

(i.e., detector array). This analyzer design closely resembles that used on the Thermo Triton TIMS and Neptune ICP-MS.

2.5. Detector array

Ions arriving at the image plane of the mass analyzer encounter a multi-collector array containing 8 pairs of detectors (one pair on each of 6 detector positions and 2 pairs at a 7th detector position), with each pair consisting of an electron multiplier and Faraday cup immediately adjacent to one another. One detector pair occupies a fixed position in the center of the detector array, while each of five detector pairs (L3, L2 and L1 at lower mass, and H1 and H2 at higher mass than the central detector) are mounted on moveable trolleys. The final two detector pairs (H3 and H4) are mounted together on a single moveable trolley, a fixed distance apart from one another. The central detector employs a large-scale secondary electron multiplier (SEM), while the others use miniaturized secondary electron detectors designed to meet the tight space requirements of a variable multicollector array. These compact ion counters are referred to as Compact Discrete Dynode SEMs, or 'CDDs'. The analyzer exit slits that define the width of each collector are 1.1 mm (for CDD's) or 1.3 mm (for Faraday cups) wide for all detector positions but H4, which has a 40 μm slit. A retarding-potential quadrupole (RPQ) lens is mounted immediately in front of the SEM at the central position, serving to reject low-energy ions that have suffered energy loss due to scattering events in route from the ion source slit to the detector or are product ions from a metastable decay of a molecular ion. The RPQ both improves abundance sensitivity and reduces background for that detector.

The system is configured such that only one detector in each pair (i.e., SEM/CDD or Faraday cup) can be used at a given time, but SEM, CDD's, and Faraday cups at different positions can be employed in any combination under computer control. Switching between SEM, CDDs and Faraday cups is controlled via electrostatic deflectors at the exit slit positioned before each detector position (which also serve to protect the CDDs from high ion currents when not in use). For all but the fixed central position, the detector trolley generally needs to be physically repositioned when switching between Faraday and SEM because the two collectors do not lie at the same place on the detector plane. The ten feedback electrometers used to register currents in the Faraday cups have nominal gains of 10^7, 3×10^8, 10^{10}, 10^{11}, and 10^{12}. They are fully multiplexed, such that any of the ten electrometers can be assigned to any of the eight Faraday cups. The components of the Ultra's detector array closely resemble those used on the Thermo Scientific Triton TIMS and Neptune ICP-MS. The flexibility of the Ultra's detector array enables quantitative analysis over a large range in signal intensity (ion currents of $\sim 2 \times 10^{-19}$ to 5×10^{-6} A) at each detector position.

The trolleys on which detector pairs are mounted (i.e., L3, L2, L1, H1, H2 and H3/4 detector pairs) are moved by a mechanical system under computer control with in situ position readout, identical to those used in the Triton TIMS and Neptune ICP-MS. This system permits maximum separation of detectors (between the Faraday cup at L3 and the EM at H4) of 150 mm, corresponding to a relative mass range of ~16% of the mass at the center position. The minimum separation between detector pairs can be varied by moving or re-positioning the CDD detectors on adjacent trolleys, between 3.5 and 10 mm (or 0.4–1.2% relative, of the mass at the center position). This minimum spacing is sufficiently large that two adjacent positions cannot simultaneously detect species sharing the same cardinal mass, but close enough to measure adjacent cardinal masses up to 80 amu for all collector configurations (above which masses must differ by 2 or more amu to be simultaneously detected for all collector configurations).

An essential capability of the Ultra's detector array is that the relative positions and detector sensitivities (both ion counting and Faraday cup current measurements) are under full user control, via the computer interface, at every mass position. The detector array can thus be reconfigured quickly, on a time scale of seconds to minutes (depending on need), without breaking vacuum. This capability is significant because many analytes of interest require comparison of measured ratios for two or more parent and/or

daughter ions. Thus, the detector array often must be reconfigured over the course of measurements made on a single sample. To maximize both precision and throughput, that reconfiguration should be rapid, accurate and convenient. For a high resolution multicollector instrument, very precise control of detector positions is required to ensure optimum peak overlap for all peaks at the same time. The reproducibility of cup positions on the Ultra is ~10 μm or less.

2.6. Vacuum system

The inlet system of the Ultra is evacuated by an oil-lubricated rotary mechanical pump for the low-vacuum waste line, and by a turbomolecular pump backed by an oil-lubricated rotary mechanical pump to reach high vacuum. Baseline pressure in the inlet system is $\sim 10^{-8}$ mbar. The ion source and analyzer are both evacuated by turbomolecular pumps backed by a dry scroll-type mechanical pump (Edwards, XDS 5). The analyzer is also evacuated by two ion pumps—one between the ESA and magnet, and one between the magnet and detector array—and the space between the source and source housing can be cryo-pumped by a liquid nitrogen cold trap to further reduce background. All major components of the inlet system, source, analyzer and detector housing can be baked at temperatures up to 200 °C. Baseline pressures in the source and analyzer are $\sim 10^{-8}$ and 10^{-9} to 10^{-10} mbar, respectively.

2.7. Computer interface

The Ultra is controlled using a modified version of Thermo Scientific Isodat software running on adesktop computer interface. This interface permits control of inlet system pneumatic valves and bellows volumes, source filament current, potentials on ion optic elements, magnet field, detector trolley positions, detector type at each position, SEM operating voltage, and the amplification of each Faraday cup electrometer. The software also records and processes signals from each detector, though most of the data reported here were processed separately using Matlab and Excel.

3. Performance characteristics

The Ultra was installed at Caltech in December 2011. Data documenting the performance characteristics of this instrument were collected between December 2011 and April 2012. The results presented here are representative of typical analytical sessions in our work to date with the Ultra.

3.1. Ion yield

The Ultra has a useful ion yield, measured for CO_2 with the widest available entrance slit (250 μm), of 1 ion per 1200 molecules introduced to the ion source. As for all EI sources, this value varies with instrument tuning, the age and condition of the filament, and the analyte gas, i.e., the ion yield for H_2 or O_2 is generally lower, while the ion yield for C_2 and larger alkanes is higher. The useful ion yield of the Ultra is approximately half that achieved by the Thermo Scientific MAT253 (all other factors being equal), reflecting the smaller entrance slit of the Ultra (250 vs. 500 μm). Useful ion yield on the Ultra decreases approximately linearly with further reduction of the entrance slit width. Thus the 16 μm slit reduces useful ion yield by a factor of ~12, and the smallest entrance slit used to date—5 μm—reduces useful ion yield by a factor of ~40. This linear inverse relationship between slit width and ion transmission is consistent with aperturing of an ion beam that is approximately homogeneous in density.

3.2. Mass range

The Ultra is capable of detecting ions with mass to charge ratios (m/z) ranging from 1 to 300 amu. This is substantially larger than the mass range possible in existing IRMSs and is a key capability for the study of volatile organic molecules and perhaps other species (e.g., fluorides, xenon).

3.3. Mass resolution

The mass resolving power of the Ultra has been measured using 250, 16 and 5 μm entrance slits, referred to here as low, medium, and high resolution, respectively. 50 and 25 μm slits are also readily available for the Ultra due to its shared heritage with the Neptune ICP-MS. It would also be straightforward to machine entrance slits having other dimensions; we anticipate that mass resolutions obtained with these alternate entrance slits will differ from those measured here roughly in proportion to the differences in width.

We use the $M/\Delta M$ definition of mass resolving power because it is most relevant to measurements made by scanning multiple ion beams of closely similar mass across a single detector that is significantly wider than each ion beam (Fig. 2). The values quoted here are representative; in practice, mass resolving power varies by ~5–10% around these values in response to a variety of instrument conditions.

The mass resolving power obtained using the lowest resolution, highest transmission entrance slit is typically ~1800. This is sufficient for separation of some isobaric interferences from common contaminants at relatively low mass, e.g., $^{16}O^+$ from $^{12}CH_4^+$ (Fig. 3). This configuration generally will not resolve isotopic isobars in organic molecules (e.g., $^{13}CH_4^+$ from $^{12}CH_3D^+$), although in some cases it is acceptable to combine such closely spaced ion beams and interpret their summed intensity through an ion correction scheme, much as measurements of mass-45 CO_2 are commonly interpreted as a combination of $^{12}C^{16}O^{17}O^+$ and $^{13}C^{16}O_2^+$ [23]. This approach has the advantages of greater speed, convenience and precision enabled by relatively high transmission. For example, we have found it is generally preferable to ion correct contributions of H+ adduct species to related isotopologues of hydrocarbons (e.g., the contribution of $^{12}CH_5^+$ to mass 17 methane isotopologues) based on their measured pressure dependence in a medium mass resolution measurement, rather than increasing mass resolution to directly resolve them (although both approaches are possible).

The medium resolution configuration (16 μm entrance slit) can reach a mass resolving power of 18,000, and is more typically 15–16,000. This resolution allows separation of many contaminant species at higher mass (e.g., $^{48}Ti^+$—a contaminant we suspect is sublimed off the source filament—from $^{12}C^{18}O_2^+$) as well as many interferences among isotopic isobars (e.g., $^{15}N^{14}N^{16}O^+$ and $^{14}N^{15}N^{16}O^+$ from $^{14}N^{14}N^{17}O^+$; Fig. 4).

The high resolution configuration (5 μm slit) can reach a mass resolving power of 27,000, and is routinely 20–25,000. This is sufficient to resolve a wide range of isobaric interferences, particularly in low- to medium-mass organic molecules and including those ions formed by H-transfer reactions during ionization, which we term 'H adducts' (e.g., discriminating $^{13}CH_3D^+$ from $^{13}CH_5^+$; Fig. 5). This resolution is also sufficient to separate some hydride interferences, such as $^{12}C^{16}O_2H^+$ with $^{13}C^{16}O_2^+$ (nominal $M/\Delta M$ of ~10,066).

3.4. System stability

System stability, defined as the standard deviation of peak position relative to a fixed detector, is 1.5 ppm over 1 h, and reflects the stability of the accelerating potential, ESA center potential, magnetic field intensity of the water cooled and temperature-controlled

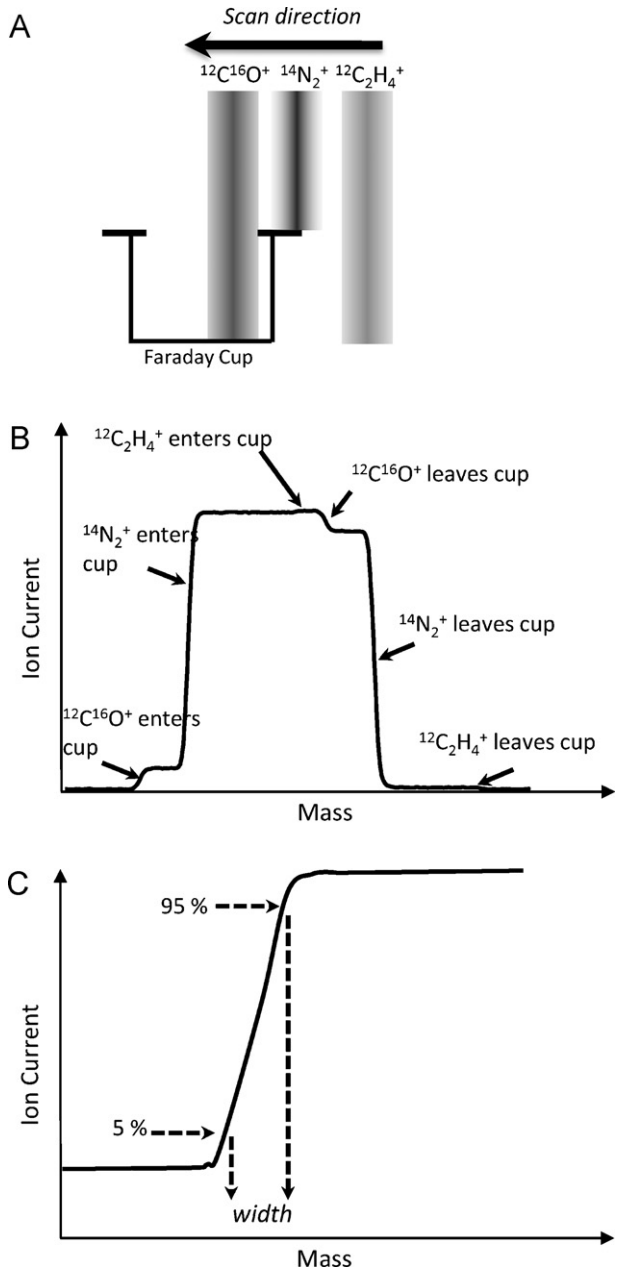

Fig. 2. Illustration of the origin and characteristics of a peak shape scan such as Figs. 2–5, and the definition of mass resolution adopted in this study. (A) A set of three ion beams sharing a cardinal mass—in this case, the three mass-28 species, $^{12}C^{16}O^+$, $^{14}N_2^+$ and $^{12}C_2H_4^+$—are translated across a detector by gradually increasing the strength of the magnetic field and thus decreasing the radii of curvature of all ion beams as they pass through the magnet. (B) A peak measured by scanning the mass 28 beam across a Faraday collector while bleeding N_2 gas into the ion source. $^{12}C^{16}O^+$ and $^{12}C_2H_4^+$ are isobaric interferences resulting from source contaminants. (C) Illustration of the measurement of ΔM in the definition of mass resolution, $M/\Delta M$, used in this study.

magnet, and—to a lesser extent—several other lens potentials. This is sufficient to obtain stable and precise measurements on small shoulders (or other features) of complex composite peaks, even when those features have an equivalent width of only a few mDa units or, in some cases, less.

3.5. Background ion currents

Johnson noise on Faraday cup signals is typically $\sim 10^{-16}$ A when measured at the highest available amplification (10^{12}) with

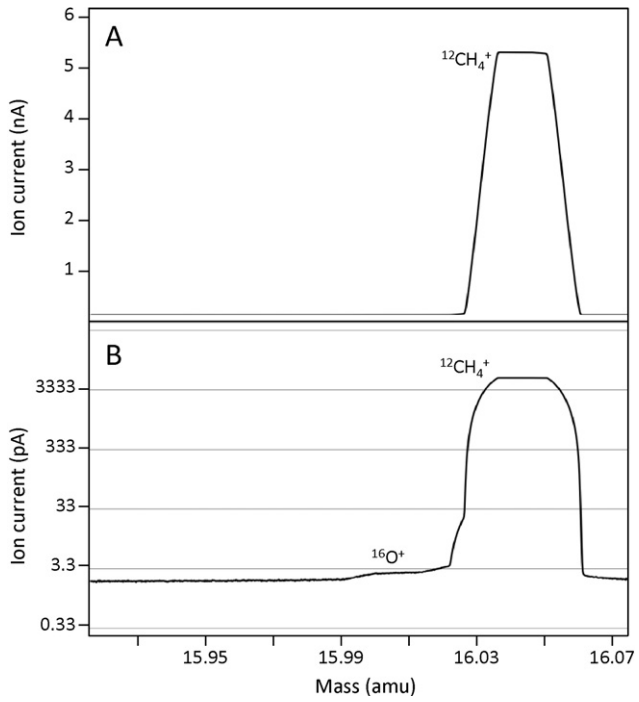

Fig. 3. Peak scan measured at m/z of 16 of methane ($^{12}CH_4^+$) and a contaminant isobaric interference of ^{16}O, using the low resolution (250 μm) entrance slit and a Faraday collector detector read through a 3×10^8 amplifier. (A) Linear scale: panel B is a logarithmic scale, which reveals the low intensity $^{16}O^+$ interference on the low-mass side of the peak. The nominal mass resolution is 1800. $^{16}O^+$ is fully resolved from $^{12}CH_4^+$ at mass positions ≥16.028 amu. Isobaric interferences from fragment ions of methane ($^{13}CH_3^+$, $^{12}CH_2D^+$, $^{13}CHD^+$, $^{12}CD_2^+$) are not visible at this resolution and sensitivity, but collectively contribute ~1% to the mass 16 beam.

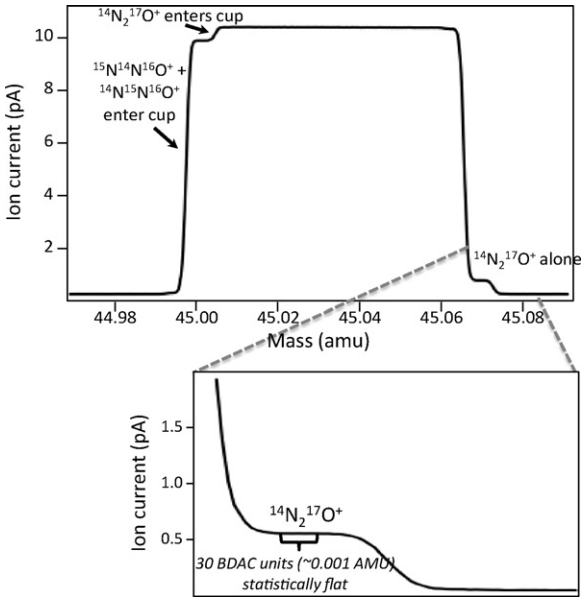

Fig. 4. Peak scan measured for mass 45 of N_2O ($^{14}N^{15}N^{16}O^+$, $^{15}N^{14}N^{16}O^+$, and $^{14}N_2{}^{17}O^+$), using the medium resolution (16 μm) entrance slit and a Faraday collector read through a 1×10^{11} amplifier. The main panel illustrates the full peak scan; the inset magnifies the high-mass side where $^{14}N_2{}^{17}O^+$ is observed. The nominal mass resolution is 17,900. $^{13}C^{16}O_2^+$ and $^{12}C^{17}O^{16}O^+$ are not visible at this scale in high purity N_2O, but create a visible third feature on the low mass side of this peak in mixed CO_2/N_2O gases. Note that the $^{14}N_2{}^{17}O^+$ ion beam can be analyzed in isolation, fully resolved from adjacent isobars, with a statistically flat 'shoulder' ~30 BDAC units wide (i.e., 30 steps in the digital controller responsible for setting the magnetic field intensity). Peak positions are generally stable to within ±1–3 BDAC units over tens of minutes.

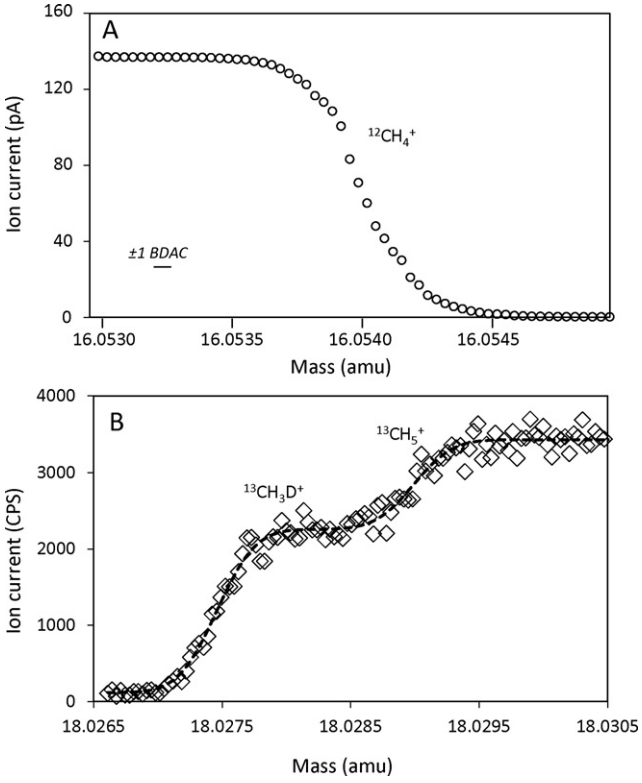

Fig. 5. Portions of scans measured for m/z 16 of CH_4 (panel A: only contributions from $^{12}CH_4^+$ visible) and m/z of CH_4^+ (panel B: only contributions from $^{13}CH_3D^+$ and $^{13}CH_5^+$ visible), using the high resolution (5 μm) entrance slit, a Faraday collector read through a 1×10^{10} amplifier for mass 16 (panel A) and an SEM detector for mass 18 (panel B). The mass resolution is 25,300 in panel A and 22,000 in panel B. Panel A illustrates that ion beams are well under 1 mDa wide using the high-resolution configuration. Panel B illustrates that that ion beams very near relatively intense isobaric interferences can be fully resolved. The $^{13}CH_3D^+$ ion beam can be analyzed in isolation, fully resolved from $^{13}CH_5^+$, with a statistically flat 'shoulder' ~15 BDAC units wide (i.e., 15 steps in the digital controller responsible for setting the magnetic field intensity). Peak positions are generally stable to within ±1–3 BDAC units over tens of minutes.

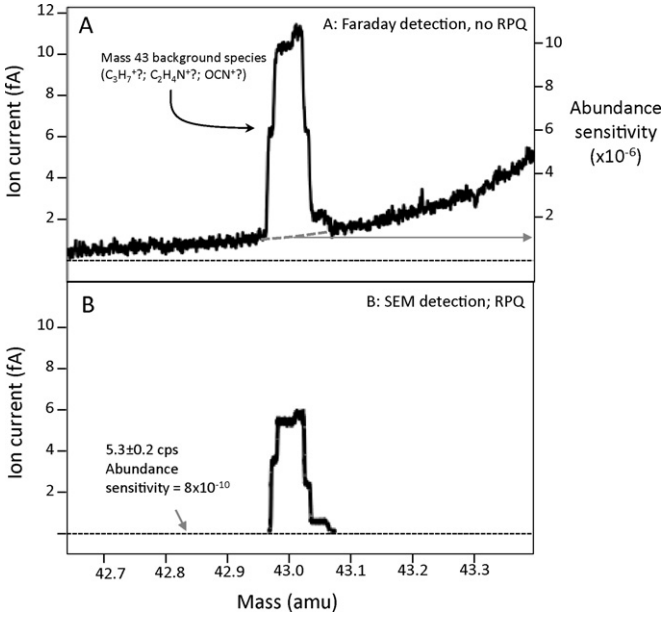

Fig. 6. Ion intensities observed near m/z of 43 in the presence of an intense (~1.07 nA) beam at m/z of 44 ($^{12}C^{16}O_2^+$). Panel A was measured with a Faraday collector registered through a 10^{12} amplifier and did not make use of the RPQ retardation lens; panel B was measured with an SEM detector and did make use of the RPQ lens. The family of peaks near m/z of 43 likely includes contributions from background hydrocarbon fragments (e.g., $^{12}C_3H_7^+$) and their isotopologues (e.g., $^{12}C_2{}^{13}CH_6^+$), and possibly other species. In panel A, the gray arrow indicates the formal abundance sensitivity at the center of the $m/z = 43$ peak. In panel B, the gray arrow indicates the location where we made a separate measurement of count rate vs. time near m/z of 42.85 amu to precisely define the abundance sensitivity in this part of the mass spectrum.

integration times of 1 s, and is generally similar to that achieved in a wide range of commercial TIMS, IRMS, and ICP-MS instruments. Dark noise on the SEM and CDD detectors varies with their operating voltage and condition, but is typically 0.004–0.01 cps.

3.6. Abundance sensitivity

The abundance sensitivity of a mass spectrometer describes the current measured by a detector due to an ion beam further away than the peak width conventionally used to describe the formal mass resolving power. Such stray ion currents arise from the broadening of nearby intense beams due to the energy distribution of individual ions caused by scattering, by decay of metastable parent ions and from ion-optical aberrations. Abundance sensitivity is typically measured as the ratio of signal intensities at a distance on the detector image plane 1 amu away from a known, intense ion beam. Naturally, this fixed mass distance translates into a wide range in *relative* mass differences across the 1–300 amu mass range of the spectrometer—in other words, the physical distance along the image plane that separates masses 1 and 2 is far larger than that which separates masses 299 and 300. Moreover, it is often useful to characterize peak tailing at distances smaller than 1 amu but larger than the formal definition of peak width (ΔM). Therefore, we present several different metrics for abundance sensitivity and, more generally, peak tailing in the Ultra.

To represent abundance sensitivity for moderate-mass ions both with and without the RPQ, we measured ion currents near m/z 43 in the presence of a 1.07 nA ion beam of $^{12}C^{16}O_2$ (Fig. 6a and b). The formal mass resolving power measured at m/z 44 during the measurement was ~18,000. The region around m/z 43 contains a family of low-intensity but detectable ions, likely a collection of background hydrocarbon species introduced either with analytes or as trace contaminants in the vacuum system. Three of these background species are visible in the magnet scan made with a Faraday cup registered through a 10^{12} amplifier with no RPQ (Fig. 6a), and a fourth is apparent in the magnet scan made with the central SEM using the RPQ lens (Fig. 6b). At least two more, very low intensity (10s of cps) peaks can be identified when the data used to construct Fig. 6b are viewed at exaggerated vertical scale. Regardless, the diffuse background on which these ions are superimposed is clear in both cases. The gently sloping ~0.5–5 fA background observed at the center of the m/z 43 beam in Fig. 6a corresponds to an abundance sensitivity of $\sim 1 \times 10^{-6}$ relative to the maximum m/z 44 ion current. This value is typical of abundance sensitivity for the Ultra at moderate mass without the RPQ. When the same mass range is measured under the same conditions but using the central SEM behind the RPQ lens (Fig. 6b), the background current drops to ~5 cps, corresponding to a formal abundance sensitivity of 8×10^{-10}.

We explored the limits of abundance sensitivity on the Ultra by studying ion currents in the vicinity of m/z 3—$^3He^+$ as well as HD^+ and H_3^+ (presumably from background H_2 and H_2O in the vacuum system)—in the presence of a large (0.3 nA) ion current of $^4He^+$ (Fig. 7). Ions were measured on the central SEM shielded by the RPQ, at positions 0.01 amu above and below the edges of the m/z 3 ion beams. The formal mass resolving power at m/z 4 in this measurement was 10,000. A dark-noise-corrected count rate of 0.007 ± 0.003 cps was observed averaging across all three

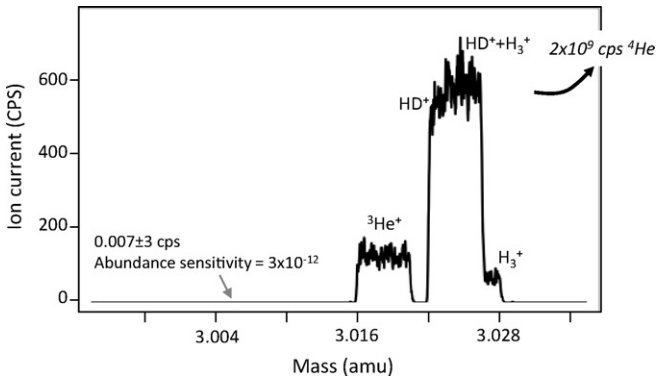

Fig. 7. Ion intensities observed near 3 amu in the presence of an intense (~10^9 cps) beam at mass 4 amu ($^4He^+$). Data were gathered using the SEM detector with the RPQ lens. Data were processed by smoothing with a sliding window 3-BDAC units wide (<0.0001 amu), and by removing a single 'spike' of signal, several tens of CPS high, that occurred at a single BDAC value between the $^3He^+$ and HD^+ peaks. Peaks are observed for $^3He^+$, HD^+ and H_3^+. The gray arrow indicates the location of one of several locations where we made separate measurements of count rate vs. time to precisely define the abundance sensitivity in this part of the mass spectrum (the other locations are off-scale to higher and lower mass; counts from all three such measurements were combined to improve the statistical confidence on the reported abundance sensitivity value).

positions where measurements were made, corresponding to an abundance sensitivity of 3×10^{-12}. This is the lowest (best) abundance sensitivity that has been reported, as far as we are aware, in any conventional sector isotope ratio mass spectrometer (i.e., TIMS, ICP-MS or IRMS). Presumably this performance is at least in part due to the large proportional mass difference between 3 and 4 amu.

We further explored the variation of ion intensity with distance along the image plane closer to (i.e., much less than 1 amu away from) relatively intense ion beams by studying m/z 3 in the presence of H_2, which yields abundant HD^+ and H_3^+ ions. These measurements are more representative of the extent of 'tailing' that occurs between ions having the same cardinal mass. A scan of ion intensity on the low-mass side of an 11.4 pA m/z 3 ion beam (composed of HD and H_3, roughly in proportion to their ratios in Fig. 6b), that was generated by introducing H_2 to the ion source (Fig. 8). The contribution of ^3He in this peak scan is inferred to be negligible (≪1 cps) based on the low measured intensity of ^4He and typical $^3He/^4He$ ratios of background and natural helium gases.

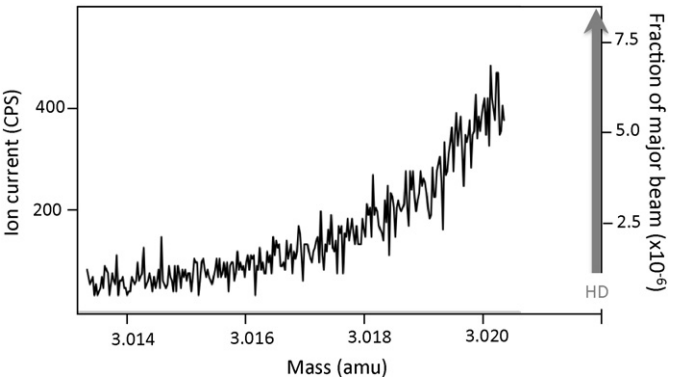

Fig. 8. Ion intensities observed near m/z 3, immediately adjacent to a relatively intense beams of HD^+ and H_3^+ (generated by delivering H_2 to the ion source), the near edge of which lies at ~3.022 amu. Data were gathered using the SEM detector with the RPQ lens. Signal resulting from peak tailing amounts to ~10^{-5} of the peak height at a distance of ~1 mDa, and drops to 10^{-6} at a distance of ~6 mDa. This is representative of the extent to which measurements of one species at a cardinal mass are influenced by contributions from nearby isobaric interferences (e.g., the relative contribution of ^{15}N isotopologues of N_2O to $^{14}N_2{}^{17}O$ in Fig. 4).

Measurements were made on the central SEM with RPQ, with a mass resolving power of 10,000. Ion intensities were measured to be ~1–5 × 10^{-6} times that of the maximum intensity of the nearby peak at a distance of ~0.002 amu from the edge of the HD^+ peak (the closest of the pair, HD^+ and H_3^+). They declined as an approximately exponential function of distance from the known peak, to a level of ~10^{-7} times the maximum over a distance along the detector image plane equivalent to ~0.005 amu. We infer that measurements made immediately adjacent to a recognized ion beam (within a few mDa) will typically contain contributions from that ion beam on the order of 10^{-5} to 10^{-7}, whereas the formal abundance sensitivity can reach 10^{-12} under ideal conditions in the He mass range (large relative mass separation and use of the RPQ).

3.7. Detection limits

The background currents and abundance sensitivity documented above suggest that the Ultra should be capable of measuring isotope ratios in the part-per-trillion range—just a few orders of magnitude greater than those accessible to accelerator mass spectrometers, at least in the low mass range of He. We tested this potential by analyzing the $^3He/^4He$ ratio of a helium sample that had been synthetically depleted in ^3He relative to natural abundance using the 'heat flash' method [24]. The natural $^3He/^4He$ ratio is 10^{-6} in air and ~10^{-7} in crustal gases. The ^4He enrichment process used to prepare the studied gas is believed to result in helium with $^3He/^4He \leq 10^{-12}$, although this had not been previously verified and we found that different aliquots of this material vary significantly in actual ^3He content. We present here results from the aliquot with lowest $^3He/^4He$ ratio, which provides the most stringent test of the Ultra's detection limits. Thirty minutes of integration on the ^3He peak, adjacent to a 0.3 nA current of ^4He, resulted in a total of 15 counts. After correction for dark noise and abundance sensitivity, this is equivalent to an upper bound on $^3He/^4He$ of 2.6×10^{-12} (95% confidence). This measurement also reflects the large dynamic range of the detector system using a combination of Faraday cups and ion counting detectors. The $^3He/^4He$ ratio of this synthetic ^4He enriched gas is not independently known. Nevertheless, concurrent measurements of tank helium from crustal sources yielded $^3He/^4He$ ratios of ~7×10^{-8}—somewhat lower than the values of 10^{-7} believed typical of such gases. We thus believe that our result may include some mass discrimination in the ion source and/or analyzer, but is still within a factor of a few of the true value. Other aliquots measured in similar fashion yielded $^3He/^4He$ ratios up to 3×10^{-10}, suggesting variance in the efficiency of ^4He enrichment. These measurements demonstrate the capability of the Ultra to make isotope ratio measurements at high source gas pressure (~10^{-7} mbar) with exceptionally low background and abundance sensitivity, and thus very low minimum detection limits.

3.8. Limits of precision

Isotope ratio measurements on the Ultra are close to counting statistics (a.k.a. 'shot noise' [25]) limits down to levels of ~0.01‰ for ratios measured with two Faraday cups, and down to ~0.1‰ for measurements using one or two electron multipliers (Fig. 9). In both cases, these levels of precision are achieved both for the 1 standard error for a single measurement (i.e., an acquisition consisting of several cycles of sample-standard comparison) and the 1 s.d. reproducibility of multiple, separate analyses of the same sample relative to a single standard. These capabilities have been demonstrated for a variety of gases (CH_4, C_2H_6, C_3H_8, CO_2, N_2O) and analytical conditions, for which representative examples are presented in Fig. 9.

Table 1
Representative expected ion intensities and precision.

Species	Abundance	Medium resolution			High resolution		
		Intensity	±1 s.e. (‰) in 100 s	Time (s) to ±0.3‰, 1 s.e.	Intensity	±1 s.e. (‰) in 100 s	Time (s) to ±0.3‰, 1 s.e.
$^{13}CH_4$	1.12E−02	31.2 pA	0.01	0.1	9.36 pA	0.02	0.4
$^{12}CH_3D$	6.23E−04	1.73 pA	0.04	2.1	0.519 pA	0.08	6.9
$^{13}CH_3D$	7.00E−06	121,000 cps	0.41	183	36,400 cps	0.74	610
$^{15}N^{14}N^{16}O$	7.32E−03	20.3 pA	0.01	0.2	6.10 pA	0.02	0.6
$^{14}N_2{}^{17}O$	3.80E−04	1.06 pA	0.06	3.4	0.316 pA	0.10	11.3
$^{14}N_2{}^{18}O$	2.01E−03	5.57 pA	0.02	0.6	1.67 pA	0.04	2.1
$^{15}N^{14}N^{18}O$	1.47E−05	254,000 cps	0.28	87.4	76,300 cps	0.51	291

'Medium' and 'high' resolution assumes a 16 and 5 μm entrance slit, respectively. All calculations assume a source pressure sufficient to produce a 33 nA beam of the major related species at low resolution. Calculated errors assume counting statistics limits for both sample and standard, each integrated for the stated time. Quoted error includes uncertainties in both sample and standard signal.

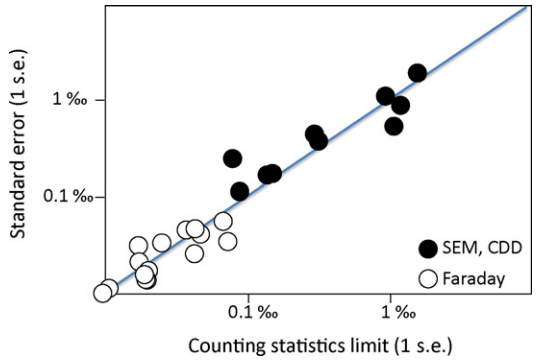

Fig. 9. Comparison of standard errors of isotope ratio acquisitions (i.e., standard deviation of cycles divided by the square root of the number of cycles, to expected errors based on shot noise limits [25]. This figure includes various isotope ratios measured on natural samples of CH_4, C_2H_6, C_3H_8, CO_2 and N_2O under a variety of different instrument resolutions and tuning conditions. Measurements made using the SEM or CDD's conform to counting statistics down to ~0.1–0.2‰, whereas measurements made with Faraday collectors conform to counting statistics down to ~0.01‰ or better.

Based on the observed performance, useful ion yield, and transmission documented above, we can predict the limits to precision for a variety of potentially interesting analyses. Table 1 gives the expected ion currents and standard errors for several analytes under typical analytical conditions and considering either the 'high' or 'medium' resolution entrance slits (5 or 16 μm, respectively). All examples assume a source pressure of $1–2 \times 10^{-7}$ mbar, yielding an ion current at low mass resolution of 30 nA for the most abundant isotopologue. For comparison, this ion current produces an equivalent 10 V signal when registered through a 3×10^8 Ω feedback resistor, as is common for the major ion beam on most IRMS instruments. The number of ions registered by a detector per unit time is reported as current down to 10^{-14} amps, approximately the lowest signal that can be background-corrected with useful precision using a Faraday cup, and as counts per second below that. We report both the standard error of a sample vs. reference gas comparison achieved in 100 s of integration, and the time of integration required to reach 0.3‰ standard error for the sample-standard comparison (i.e., $2^{0.5}$ times the counting statistics limit to precision for the sample ions). Precision better than ~0.5‰ is anticipated for a wide range of analytical targets with integration times of minutes.

4. Discussion

The Ultra has been developed utilizing components of existing and relatively well-understood mass spectrometers, but this combination results in several distinctive capabilities, some of which might not be expected based on previous instruments. For example, the Ultra routinely achieves mass resolution ~2-fold better than that of the Neptune ICP-MS, even though their mass analyzers are nearly identical. We suspect this improvement is mainly due to the intrinsic stability of the Nier-type EI ion source and the narrow range in energy and angular distribution of ions it produces. Regardless, this is an essential capability of the Ultra, because a large range of applications that are impossible with a mass resolving power of ~10,000 become feasible at ~20,000.

Similarly, the abundance sensitivity achieved by the Thermo Scientific Neptune is specified at $<5 \times 10^{-7}$ for adjacent masses of U, whereas the minimum value documented here for the Ultra is 3×10^{-12} for adjacent masses of He. It should be noted that the specification for the Neptune is an upper bound, and was measured at far higher absolute mass—and thus smaller relative mass difference—than the helium measurements in Fig. 7. It is possible that abundance sensitivity at low mass on the Neptune or similar instruments would also be in the range of 10^{-12}, though the diffuse background of Ar^+ ions in plasma source mass spectrometers may significantly degrade this. Regardless, this capability on the Ultra is orders of magnitude better than the abundance sensitivity of existing gas source IRMSs and—when combined with low-baseline EMs—enables the study of a wide range of low abundance isotopic species.

The Ultra can measure isotope ratios using one or more electron multipliers with precision approaching 0.1‰ (Fig. 9), roughly an order of magnitude better than that achieved for comparable measurements on TIMS, ICP-MS, and ion probe instruments (e.g., [26]). The limitation to precision imposed by the use of EMs can generally be attributed to drift in EM gain over time scales of minutes or longer. We suggest that the improved capabilities we observe for similar detectors on the Ultra reflect the practice of frequent (<30 s) sample/standard comparison, wherein each standard—sample—standard bracket effectively corrects for drift in the relative gains of the detectors (much as the initial introduction of sample/standard bracketing in early gas source mass spectrometers helped compensate for drift in amplifier gain). Moreover, any effect of non-linearity in detector gain is minimized by the careful intensity matching of gas source isotope ratio mass spectrometers. Thus, it appears likely that drift in SEM gain over tens of seconds is roughly an order of magnitude less than that over tens of minutes, the typical separation between sample/standard comparisons in carrier-gas applications of IRMS, and in most other kinds of mass spectrometry. Whatever the cause, it is a significant improvement that enables measurement of very low intensity ion beams with sub-per mil precision.

4.1. Tradeoffs in measurement optimization on the Ultra

The flexibility inherent in the design of the Ultra presents the analyst with several important tradeoffs that must be considered when designing and optimizing measurement strategies. First and foremost is the tradeoff between mass resolution and

sensitivity—because higher resolution is achieved via smaller mechanical apertures, it inherently results in lowered transmission and sensitivity. Most analytical targets of conventional IRMS instruments generate relatively high ion currents for all isotopologues of interest (and are measurable on Faraday cups). Consequently, measurements are generally not limited by counting statistics or detector sensitivity and stability. In these cases, transmission can be reduced markedly without meaningful degradation in the quality of measurements. The presence of SEM detectors at every detector position in the Ultra further reduces the importance of transmission for many applications, allowing operation at very high mass resolution. On the other hand, new analytes targeted by the Ultra, e.g., multiply substituted isotopologues, generally generate far lower ion currents and in these cases sacrificing mass resolution for increased transmission may be desirable.

The second tradeoff to consider is that between counting time and sensitivity. The EI sources of IRMS instruments, including the Ultra, are very stable as compared to thermal and plasma sources and sample-standard comparisons are frequent, making it is possible to achieve high precision at low ion currents simply by integrating for increased time periods. A current example of this approach is the analysis of $^{13}C^{16}O^{18}O/^{12}C^{16}O_2$ ratios, which are on the order of 5×10^{-5} in natural CO_2 but can be analyzed with precision of ~0.01‰ using a conventional Thermo IRMS-253 with sufficient patience (~2 h) [13]. This leads us to conclude that time can be traded for useful ion yield in many applications without meaningful loss of precision and accuracy. The chief drawback to such an approach is the obvious limitation to sample throughput created by long integration times.

These tradeoffs notwithstanding, we can envision some analytical targets that require exceptionally high mass resolution, yet are so rare and/or demand such high precision that they cannot be analyzed with the low transmission that results from a narrow entrance slit. We have not yet encountered any cases that could not be addressed through changes of source pressure, integration time, or other parameters, but it seems inevitable that these limitations will be encountered. Examples might include triply substituted isotopologues (e.g., $^{12}CD_3H$) or doubly substituted versions of very low abundance fragment ions (e.g., the $^{13}CD^+$ fragment of some organic compounds). It is possible that precise measurements of some such species in natural-abundance materials will remain outside the analytical window of the Ultra.

4.2. Illustrative potential applications

The capabilities of the Ultra permit a large range of isotopic analyses, including all standard IRMS measurements currently made and a wide variety of new analytes, particularly hydrocarbons. The following paragraphs briefly describe three applications that illustrate the capabilities and limitations of the instrument.

4.2.1. D_2 in molecular hydrogen

The equilibrium between $H_2 + D_2 = 2HD$ is one of the first homogeneous isotope exchange phenomena considered by Urey and colleagues (reviewed in [27]). The equilibrium strongly favors the reactants (i.e., 'clumping' of D into a doubly substituted molecule) at moderate temperatures, and the equilibrium constant exhibits remarkable temperature sensitivity (~1‰ per °C near earth surface temperatures). Thus, it could serve as a geothermometer for reducing environments in which H_2 is a constituent of the vapor phase. D_2 is also distinctively fractionated from H_2 and HD during reaction with OH, and could serve as a distinctive tracer for photochemical processing of molecular hydrogen in the atmosphere [28]. D_2 is mass-resolved from its principle isobaric interference, ^{4}He, at a resolution of 156—obviously well within the capabilities of the Ultra even in its lowest resolution/highest transmission configuration. Resolution of D_2^+ from H_2D^+ and H_4^+ (a generally unexpected species, though one we have nevertheless observed [29,30]) requires resolution of ~2600, and thus some reduction in entrance slit width is needed to measure D_2 free of any isobaric interference. Considering the tradeoffs described above, we suggest the best approach is to use a 50 μm entrance slit, with an expected mass resolution of 6000–8000. In this configuration, a typical sample will generate ion intensities of several nA for H_2^+, 1 pA for HD^+ (both easily measured by Faraday cups), and ~500 cps for D_2^+ (i.e., a peak shape and intensity similar to that of $^3He^+$ in Fig. 7b). This counting rate yields a counting-statistics limit to precision of 2‰ with ~10 min of integration. Note this measurement requires dynamic peak hopping due to the large proportional difference in mass between H_2, HD and D_2.

4.2.2. Clumped isotope analysis of N_2O

The biogeochemical and photochemical budgets of N_2O are studied through measurements of $\delta^{15}N$, $\delta^{18}O$, $\delta^{17}O$ and position-specific nitrogen isotope analysis (i.e., comparison of the α and β nitrogen sites) (e.g., [15,31]). Despite this diversity of isotopic proxies, some important components of the N_2O cycle remain under-constrained (e.g., the contribution of archea to the marine N_2O source), thus there is a need for yet more information. Multiply substituted species of N_2O (e.g., $^{15}N^{14}N^{18}O$ and $^{14}N^{15}N^{18}O$) are well suited for analysis by the Ultra and are attractive targets for improving our understanding of the nitrogen cycle. The isotopologues $^{15}N^{14}N^{18}O$ and $^{14}N^{15}N^{18}O$ are identical in mass (47.0023 amu) and are closely adjacent to the isotopic isobar $^{15}N_2{}^{17}O$ (46.9993 amu). Mass resolution of 15,700 is required to formally separate the doubly substituted species from this triply substituted, very rare isobar. The Ultra's highest resolution configuration should permit near separation of this isobar, with an estimated contribution of $\sim 10^{-4}$ of the $^{15}N_2{}^{17}O^+$ beam at m/z 47.0023 amu based on studies of abundance sensitivity and beam 'tailing' (Figs. 7 and 8). At natural isotope abundances, this amounts to only $\sim 5 \times 10^{-8}$ of the intensity of $[^{15}N^{14}N^{18}O^+ + {}^{14}N^{15}N^{18}O^+]$—a negligible contribution. In order to distinguish $^{15}N^{14}N^{18}O$ from $^{14}N^{15}N^{18}O$, it is necessary to analyze the isotopic composition of NO^+ fragment ions, just as is done in conventional position-specific ^{15}N measurements of N_2O [15]. These fragment ions are resolved from their relevant O_2 isobars ($^{16}O_2$ and $^{17}O^{16}O$) at resolving powers of 2600 and 6300, respectively—well below the resolution achieved with the narrowest entrance slit on the Ultra. Assuming normal source pressure and ion yield for N_2O, all of these species are measurable at signal intensities of ~0.1 pA or greater.

4.2.3. Position-specific C isotope analysis of propane

The data presented in Figs. 5 and 9 and Table 1 suggest the Ultra is capable of precisely measuring the C and H isotopic compositions of hydrocarbons despite the general complexity of their mass spectra (i.e., considering fragmentation, H-adduct ions created in the EI source, and isotopic substitutions of either ^{13}C or D). The potential for making clumped isotope measurements is apparent from the high resolution scan of mass-18 isotopologues of methane, which reveals a well resolved $^{13}CH_3D^+$ peak with an intensity that yields precision <1‰ over an integration time of tens of minutes (Fig. 5; medium resolution measurements that employ a pressure-dependent adduct correction may mitigate the loss in transmission at high resolution). Here we consider another, complementary measurement enabled by the Ultra: position-specific analysis of the carbon and/or hydrogen isotopic compositions of organic compounds. The approach is conceptually similar to that previously used for position-specific ^{15}N analysis of N_2O. The isotopic compositions of the intact molecular ion and of a fragment ion that preferentially samples one structural site are measured,

and the fractionation between the measured fragment and other sites in the molecular structure are calculated by mass balance.

As one example, we consider the position-specific carbon isotope analysis of *n*-propane (C_3H_8). Propane contains two structurally equivalent terminal methyl (CH_3) groups joined to a central methylene (CH_2) carbon. When introduced to an EI source and bombarded with ~70 eV electrons, propane produces a distinctive spectrum of molecular and fragment ions, including $C_1H_n^+$, $C_2H_n^+$ and $C_3H_n^+$ species (NIST Chemistry Web Book; http://webbook.nist.gov/chemistry). The singly substituted, ^{13}C isotopologues of these fragments can generally be mass-resolved from species with 1 additional H atom at a resolution that is achievable by the Ultra, e.g., the $^{13}C^{12}C_2$ fragment ion is resolved from $^{12}C_3H$ at a resolving power of ~8300. Moreover, the use of EMs on the Ultra would enable measurements of isotopically substituted versions of low-abundance fragments at the highest mass resolution, yielding ion currents equivalent to $10^{4–5}$ of cps (or greater). Thus, the $^{13}C/^{12}C$ ratio of any of the ~15 fragment and molecular ions present in the propane mass spectrum could be effectively measured.

The preceding example assumes that re-combination of fragment ions in the ion source (which will scramble the internal C-isotopic ordering of propane) is a stable, reproducible phenomenon and can be experimentally calibrated and corrected for (much as ion source 'scrambling' corrections are currently applied to measurements of position-specific ^{15}N content of N_2O and abundance of $^{13}C^{18}O^{16}O$ in CO_2). The dominant products of EI ionization of small alkanes are simple fragments so we expect this to be a second order correction rather than principal control on measured isotopic compositions of various molecular and fragment ions ([32]; with the possible exceptions of H-free species, which we suspect may include abundant recombination products). This will need to be experimentally verified. Assuming such effects are negligible or suitable for empirical corrections, measurements of the $^{13}C/^{12}C$ ratios of any two fragment ions that differ in their carbon number (e.g., CH_3 and C_2H_5) should permit calculation of the difference in $\delta^{13}C$ between the methyl and central carbon positions by mass balance.

4.3. Summary and prospects

The Ultra was designed with the general purpose of exploring the isotopic anatomies of a wide range of volatile and semi-volatile compounds—principally, but not exclusively, organics—through direct, mass-resolved measurements of singly and multiply substituted isotopologues of these molecules and their fragments. This capability is a straightforward extrapolation of many existing mass spectrometric capabilities, but its distinctive combination of acceptable analytes (molecules and their fragments) and capabilities (high resolution, abundance sensitivity, low noise ion counting detectors, moveable collectors, and demonstrated sensitivity and precision) opens up a broad array of new measurements. Mass resolving powers up to 27,000 enable separation of isobaric interferences from a wide range of contaminants and isotopic isobars; abundance sensitivity down to $\sim10^{-12}$ and dynamic range of signal intensity up to $\sim10^{13}$ enable analysis of rare multiply substituted molecular and fragment ions; and precision in isotope ratio measurements on the order of 0.1–0.01 per mil permits study of subtle natural isotopic variations.

Isotope ratio measurements have previously focused on a relatively small number of analytical targets, i.e., one to a few ion intensity ratios of elements (for TIMS, ICP and SIMS) and a handful of volatile molecules (for IRMS). The Ultra, or any broadly similar high-resolution, multi-collector isotope-ratio mass spectrometer, has the potential to expand greatly this diversity of analytes. Low molecular weight volatile organic compounds can have hundreds to thousands of isotopologues, many of which can be separated from isobaric interferences with a resolving power of ~10–20,000, and which are abundant enough to consider as plausible analytes—for example, even if one restricts oneself to the most easily analyzed singly and doubly substituted isotopologues of propane and its fragments, it will likely be possible to constrain proportions of 15 independent species ($^{13}CH_3—^{12}CH_2—^{12}CH_3$, $^{12}CH_2D—^{12}CHD—^{12}CH_3$, $^{12}CH_3—^{13}CH_2—^{12}CH_2D$, etc.), and even if one restricted oneself to the highly volatile hydrocarbons that can be introduced to the ion source without the aid of a carrier gas, there are at least a dozen compounds for which one could expect much the same diversity of analytical targets. Recent experience with clumped isotope and position-specific isotopic measurements of simple molecules (i.e., CO_2 [33] and N_2O [15]) suggests we should expect such measurements will create a wide range of novel geochemical and forensic tools.

Acknowledgements

The Ultra prototype mass spectrometer received partial funding from the NSF-EAR Instruments and Facilities program and from the California Institute of Technology. Some of the illustrative data presented in this paper was generated as part of an applied research project funded by Petrobras. Additional funding to support components of this work came from an NSF Graduate Fellowship and postdoctoral fellowship funding from the California Institute of Technology. We thank Nami Kitchen for assistance in the laboratories for stable isotope geochemistry at Caltech, and the staff at Thermo Scientific, including Chuck Douthitt, Frank Heine, Thomas Heise, Andreas Hilkert, and Silke Seedorf, for their commitment to the construction of the Ultra. We thank Ken Farley for providing samples of helium analyzed as part of this study.

References

[1] W. Dansgaard, Stable isotopes in precipitation, Tellus 16 (1964) 436–468.
[2] B.J. Peterson, B. Frey, Stable isotopes in ecosystem studies, Annual Review of Ecology and Systematics 18 (1987) 293–320.
[3] T.J. Barstow, D.M. Cooper, S. Epstein, K. Wasserman, Changes in breath ($^{13}CO_2/^{12}CO_2$) consequent to exercise and hypoxia, Journal of Applied Physiology 66 (1989) 936–942.
[4] J. Zachos, M. Pagani, L. Sloan, E. Thomas, K. Billups, Trends, rhythms and aberrations in global climate 65 Ma to present, Science 292 (2001) 686–693.
[5] S. Benson, C. Lennard, P. Maynard, C. Roux, Forensic applications of isotope ratio mass spectrometry – a review, Forensic Science International 157 (2006) 1–22.
[6] J.R. Ehleringer, G.J. Bowen, L.A. Chesson, A.G. West, D.W. Podlesak, T.E. Cerling, Hydrogen and oxygen isotope ratios in human hair are related to geography, Proceedings of the National Academy of Sciences of the United States of America 105 (2008) 2788–2793.
[7] A.O. Nier, A redetermination of the relative abundances of the isotopes of carbon, nitrogen, oxygen, argon and potassium, Physical Review 77 (1950) 789–793.
[8] C.R. McKinney, J.M. McCrea, S. Epstein, H.A. Allen, H.C. Urey, Improvements in mass spectrometers for the measurement of small differences in isotope abundance ratios, Review of Scientific Instruments 21 (1950) 724–730.
[9] B. Luz, E. Barkan, M.L. Bender, M.H. Thiemens, K.A. Boering, Triple-isotope composition of atmospheric oxygen as a tracer of biosphere productivity, Nature 400 (1999) 547–550.
[10] J.P. Severinghaus, A. Grachev, B. Luz, N. Caillon, A method for precise measurement of argon 40/36 and krypton/argon ratios in trapped air in polar ice with applications to past firm thickness and climate change in Greenland and at Siple Dome, Antarctica, Geochimica et Cosmochimica Acta 67 (2003) 325–342.
[11] D.E. Matthews, J.M. Hayes, Isotope ratio monitoring gas chromatography mass spectrometry, Analytical Chemistry 50 (1978) 1465–1473.
[12] J.M. Eiler, E. Schauble, $^{18}O—^{13}C—^{16}O$ in Earth's atmosphere, Geochimica et Cosmochimica Acta 68 (2004) 4767–4777.
[13] J.M. Eiler, Clumped Isotope geochemistry – the study of naturally-occurring, multiply-substituted isotopologues, Earth and Planetary Science Letters 262 (2007) 309–327.
[14] A. Amrani, A.L. Sessions, J.F. Adkins, Compound-specific $\delta^{34}S$ analysis of volatile organics by coupled GC/Multicollector ICPMS, Analytical Chemistry 81 (2009) 9027–9034.
[15] N. Yoshida, S. Toyoda, Constraining the atmospheric N_2O budget from intramolecular site preference in N_2O isotopomers, Nature 405 (2000) 330–334.

[16] Q.Z. Hu, R.J. Noll, H.U. Li, A. Makarov, M. Hardman, R.G. Cooks, The orbitrap: a new mass spectrometer, Journal of Mass Spectrometry 40 (2005) 430–443.
[17] D.R. Bowling, S.D. Sargent, B.D. Tanner, J.R. Ehleringer, Tunable diode laser absorption spectroscopy for stable isotope studies of ecosystem–atmosphere CO_2 exchange, Agricultural and Forest Meteorology 118 (2003) 1–19.
[18] G.J. Martin, M.L. Martin, Deuterium labeling at the natural abundance level as studied by high-field quantitative ^{2}H NMR, Tetrahedron Letters 22 (1981) 3525–3528.
[19] R. Robins, I. Billault, J. Duan, S. Guiet, S. Pionnier, B.-L. Zhang, Measurement of 2H distribution in natural products by quantitative ^{2}H NMR: an approach to understanding metabolism and enzyme mechanism? Phytochemistry Reviews 2 (2003) 87–102.
[20] A. Gilbert, V. Silvestre, R. Robins, G. Remaud, Accurate quantitative isotopic ^{13}C NMR spectroscopy for the determination of the intramolecular distribution of ^{13}C in glucose at natural abundance, Analytical Chemistry 81 (2009) 8978–8985.
[21] G.S. Remaud, Y.L. Martin, G.G. Martin, G.L. Martin, Detection of sophisticated adulterations of natural vanilla flavors and extracts: application of the SNIF-NMR method to vanillin and p-hydroxybenzaldehyde, Journal of Agricultural and Food Chemistry 45 (1997) 859–866.
[22] K.W. Huntington, J.M. Eiler, H.P. Affek, et al., Methods and limitations of 'clumped' CO_2 isotope (Delta(47)) analysis by gas-source isotope ratio mass spectrometry, Journal of Mass Spectrometry 44 (2009) 1318–1329.
[23] J. Santrock, S.A. Studley, J.M. Hayes, Isotopic analyses based on the mass spectrum of carbon dioxide, Analytical Chemistry 57 (1985) 1444–1448.
[24] P.V.E. McClintock, An apparatus for preparing isotopically pure ^{4}He, Cryogenics 1978 (1978) 201–208.
[25] J.M. Hayes, Practice and principles of isotopic measurements in organic geochemistry, a privately distributed revision of a chapter of the same name appearing in: W.G. Meinschein (Ed.), Organic Geochemistry of Contemporaneous and Ancient Sediments, published in 1983 by the Great Lakes Section of the Society of Economic Paleontologists and Mineralogists, 2002, pp. 5-1–5-31. Available at: http://www.gps.caltech.edu/~als/research-articles/other_stuff/
[26] N.T. Kita, T. Ushikubo, B. Fu, J.W. Valley, High precision SIMS oxygen isotope analysis and the effect of sample topography, Chemical Geology 264 (2009) 43–57.
[27] H.C. Urey, The thermodynamic properties of isotopic substances, Journal of the Chemical Society 1947 (1947) 562–581.
[28] R.K. Talukdar, A.R. Ravishankara, Rate coefficients for $O^D + H_2$, D_2, HD reactions and H atom yield in O^D + HD reaction, Chemical Physics Letters 253 (1996) 177–183.
[29] N.J. Kirchner, J.R. Gilbert, M.T. Bowers, The first experimental observation of stable H_4^+ ions, Chemical Physics Letters 106 (1984) 7–12.
[30] A. Alijah, A.J.C. Varandas, H_4^+: what do we know about it? Journal of Chemical Physics 129 (2008) (Art No. 034303).
[31] K.R. Kim, H. Craig, ^{15}N and ^{18}O characteristics of nitrous oxide – a global perspective, Science 262 (1993) 1855–1857.
[32] R.M. Silverstein, F.X. Webster, D.J. Kiemle, Spectrometric Identification of Organic Compounds, Wiley & Sons, 2005, 502 pp., ISBN 978-471-39362-7.
[33] J.M. Eiler, Paleoclimate reconstruction using carbonate clumped isotope thermometry, Quaternary Science Reviews 30 (2011) 3575–3588.